nature biotechnology

Expansion and patterning of cardiovascular progenitors derived from human pluripotent stem cells

Matthew J Birket[1], Marcelo C Ribeiro[1], Arie O Verkerk[2], Dorien Ward[1], Ana Rita Leitoguinho[1], Sabine C den Hartogh[1], Valeria V Orlova[1], Harsha D Devalla[1], Verena Schwach[1], Milena Bellin[1], Robert Passier[1] & Christine L Mummery[1]

The inability of multipotent cardiovascular progenitor cells (CPCs) to undergo multiple divisions in culture has precluded stable expansion of precursors of cardiomyocytes and vascular cells. This contrasts with neural progenitors, which can be expanded robustly and are a renewable source of their derivatives. Here we use human pluripotent stem cells bearing a cardiac lineage reporter to show that regulated *MYC* expression enables robust expansion of CPCs with insulin-like growth factor-1 (IGF-1) and a hedgehog pathway agonist. The CPCs can be patterned with morphogens, recreating features of heart field assignment, and controllably differentiated to relatively pure populations of pacemaker-like or ventricular-like cardiomyocytes. The cells are clonogenic and can be expanded for >40 population doublings while retaining the ability to differentiate into cardiomyocytes and vascular cells. Access to CPCs will allow precise recreation of elements of heart development *in vitro* and facilitate investigation of the molecular basis of cardiac fate determination. This technology is applicable for cardiac disease modeling, toxicology studies and tissue engineering.

Human pluripotent stem cells (hPSCs) can recapitulate aspects of development *in vitro* and produce cell types not routinely available from primary tissue. This has already proven useful in modeling disease, screening compound libraries to identify drug targets and developing cell therapies[1–3]. The heart is of particular relevance because of its vital function and inaccessibility. Differentiation of hPSCs to cardiomyocytes and vascular cells can contribute to understanding the nature of congenital defects in development and disease and in safety pharmacology, as the heart is a crucial target of toxicity[4]. The availability of expandable hPSC-derived multipotent CPCs with the ability to form cardiomyocytes and vascular cells in culture could advance all of these areas by providing renewable precursors without the need to return to the hPSC source. This goal has been challenging because the culture requirements of CPCs are uncertain and their molecular identity is poorly defined[5].

In heart development, CPC populations arise within bilateral cardiogenic areas of mesoderm. Following prior lineage segregation, one CPC population, called the first heart field (FHF), forms the myocardium of the linear heart tube, and the remaining pool of undifferentiated CPCs, called the second heart field (SHF), are added later, providing further cardiomyocytes, smooth muscle and endothelial cells to the developing heart[6]. The genes *ISL1* and *NKX2-5* (the vertebrate homolog to *tinman*), which encode homeobox transcription factors, are two of the earliest genes identifying CPCs and may be expressed at least transiently in the majority of these cells[7–9]. Both have been used to isolate multipotent CPCs from embryonic or neonatal hearts and hPSCs, and the potential of these cells for differentiation has been demonstrated in short-term experiments[10–12]. However, the difference between the isolated populations in these respective studies is unclear, and heterogeneity in clonal experiments suggests that there is a need for additional markers and better methods for robustly maintaining discrete populations at different stages of commitment. Expression of *Nkx2-5* in mice, for example, is present in the majority of CPCs destined to form 'working' myocardium but is thought to be absent in the SHF lineage destined for the sinoatrial node (SAN)[13]. These SAN progenitors, however, express *Isl1* and may also express *Tbx18*, which encodes a T-box transcription factor[14]. Conversely, in mice, the FHF CPC population, which gives rise mainly to primitive left ventricular progenitors, may be uniquely marked by early *Hcn4* expression[15,16]. *Hcn4* is expressed later and then maintained in the Isl1^{+}Nkx2-5^{-}Tbx18^{+} SHF-CPC–derived SAN. These important commitment steps and their regulatory mechanisms are not resolved in the hPSC model. Generating pure populations of pacemaker cells is crucial for modeling sinus node dysfunction and could be useful in the future development of biological pacemakers; pure populations of ventricular or atrial working myocardial cells would similarly benefit other applications.

The practical challenge for more effectively directing cardiac progression from hPSCs is to slow the otherwise rapid and uncontrolled transition from the appearance of CPCs, marked by increasing expression of platelet-derived growth factor receptor-α (PDGFR-α)[17], to their differentiation, predominantly to cardiomyocytes of heterogeneous identity. Here, taking advantage of *NKX2-5*$^{eGFP/w}$ human embryonic stem cells (hESCs) in which the emergence of NKX2-5^{+} cells can be followed by eGFP expression, we report a solution through

[1]Leiden University Medical Center, Leiden, the Netherlands. [2]Amsterdam Medical Center, Amsterdam, the Netherlands. Correspondence should be addressed to C.L.M. (c.l.mummery@lumc.nl).

Received 23 January; accepted 2 June; published online 20 July 2015; doi:10.1038/nbt.3271

regulated MYC expression. This enables the expansion of primitive pre–*NKX2-5*$^+$ CPCs, their patterning through regulation of fibroblast growth factor (FGF) and bone morphogenetic protein (BMP) signaling and their directed differentiation to NKX2-5–eGFP$^+$ working ventricular-like cells, NKX2-5–eGFP$^-$ pacemaker-like cells and endothelial and, later, smooth muscle cells, mimicking the cardiac developmental program.

RESULTS

Regulated MYC expression restrains cardiac differentiation

A doxycycline-inducible *MYC* transgene (Tet-On-*MYC*) was introduced into an *NKX2-5*$^{eGFP/w}$ hESC line to allow *MYC* expression to be controlled during differentiation. In *NKX2-5*$^{eGFP/w}$ Tet-On-*MYC* hESCs and day 5 embryoid bodies (EBs) derived from them, *MYC* expression could be tightly regulated by doxycycline (dox) (**Fig. 1a**,**b** and **Supplementary Fig. 1**). High transgene expression was also evident given the autosuppression of endogenous *MYC*[18]. In the absence of dox these hESCs could differentiate to beating cardiomyocytes in EBs with similar efficiency as the parent line, making ~60% eGFP$^+$ cells by day 9 of differentiation (**Supplementary Fig. 2a**,**b**). Activation of *MYC* expression by addition of dox during cardiac differentiation at day 5.5 or beyond had little impact on the expression of NKX2-5–eGFP (**Supplementary Fig. 2c**), whereas dox addition at day 4.75 significantly blocked differentiation from the PDGFR-α$^+$ state to the NKX2-5–eGFP$^+$ state (**Fig. 1c**,**e** and **Supplementary Fig. 2e**). There was no such effect of dox on eGFP expression in the parent line (**Supplementary Fig. 2b**). We also analyzed the expression kinetics of the posterior heart field marker podoplanin (PDPN) (**Supplementary Fig. 2d**). PDPN was highly expressed in undifferentiated hESCs and was maintained in derivative NKX2-5–eGFP$^+$ cardiomyocytes, whereas in the heart myocardium PDPN expression is restricted largely to the SAN[19]. These data suggest that PDPN may have utility as a marker of both primitive CPCs and SAN-like derivatives in this system.

With the aim of further restricting CPC differentiation–inducing signaling, we added SB431542 (SB) together with dox to inhibit endogenous transforming growth factor-β (TGF-β)–activin signaling; this further restrained NKX2-5–eGFP induction as measured on day 8 (**Fig. 1d**,**e**).

CPCs proliferate with defined mitogenic stimulation

To investigate the proliferative capacity of this largely PDGFR-α$^+$, pre–NKX2-5$^+$, putative CPC-encompassing population, we seeded cells at day 6 of EB differentiation at low density on a soft basement membrane. With maintained *MYC* expression in the continued presence of dox, cells proliferated to form small spheres (**Fig. 1f**). If dox was not added or was removed on seeding, spheres did not form, and cell proliferation was not apparent on this substrate. Yet dox combined with SB was insufficient to robustly sustain the culture in a growing state beyond this first expansion, so additional mitogenic stimulants or supportive factors were sought.

Roles have been proposed for IGF-1 and hedgehog signaling in CPC proliferation during cardiac development[20,21]. Dox combined with SB and IGF-1 or SAG (an agonist of Smoothened, part of the hedgehog signaling pathway) increased proliferation within spheres by 2.1-fold or 2.7-fold, respectively (**Fig. 1f**,**g**). Whereas dox combined with SB, IGF-1 and SAG had an additive effect, increasing proliferation by 4.1-fold, MYC remained essential. The expression of SAG-induced hedgehog response genes *GLI1* and *PTCH1* was not modified by IGF-1, suggesting that the additive potentiation was not due to enhanced hedgehog signaling (**Fig. 1h**). Time-lapse imaging showed that spheres were typically clonal (**Fig. 1i** and **Supplementary Video 1**) and remained NKX2-5–eGFP$^-$ under these conditions.

Concerted FGF and BMP signaling induce *NKX2-5* expression

As these sphere-forming cells might be in a developmental state equivalent to pre–NKX2-5$^+$ CPCs, we tested whether expression of *NKX2-5*–eGFP could be induced in this population by FGF and BMP signaling, as occurs during heart development[22–26]. For this experiment, spheres were generated in medium containing dox, SB, IGF-1 and SAG (DSIS) in the presence or absence of basic FGF (bFGF) and/or BMP4. SB does not interfere with BMP signaling[27]. After 6 d, bFGF had potently induced NKX2-5–eGFP expression in a concentration-dependent manner yet also reduced the number of spheres formed (**Fig. 2a**–**d**). BMP4 alone had little impact on NKX2-5–eGFP expression but markedly potentiated induction by bFGF and, when combined with 1 ng/ml bFGF, was sufficient to induce NKX2-5–eGFP expression in >95% of cells and to a higher intensity. BMP4 in combination with bFGF also increased sphere formation compared to bFGF alone (**Fig. 2c**). Inhibition of BMP signaling with dorsomophin-homolog 1 (DMH1) restricted NKX2-5–eGFP induction by bFGF and completely blocked sphere formation at higher concentrations of bFGF. A time-course experiment showed eGFP expression after 48 h of exposure to bFGF and BMP4, and this expression reverted on factor withdrawal (**Supplementary Fig. 3**). Both the CPC marker PDGFR-α and the primitive CPC–SAN marker PDPN were downregulated with increasing concentrations of bFGF and BMP4, creating heterogeneity in addition to the variation in NKX2-5–eGFP levels (**Fig. 2a**,**b**).

To additionally suppress endogenous FGF signaling and minimize differentiation, we produced NKX2-5-eGFP$^-$PDPN$^+$ spheres in the presence of an FGF receptor inhibitor (SU5402) as well as DMH1 (**Fig. 2e**). Differences in NKX2-5 expression were confirmed by western blotting (**Fig. 2f** and **Supplementary Fig. 4**). **Figure 2g** shows an analysis of surface markers in NKX2-5–eGFP$^-$PDPN$^+$ cells expanded in DSIS with SU5402 and DMH1, compared to the most divergent NKX2-5–eGFP$^+$ cells expanded in DSIS with 1 ng/ml bFGF and BMP4. The pluripotent markers TRA160 and E-cadherin were absent, as were vascular endothelial growth factor receptor 2 (VEGFR2, here referred to as KDR) and stem cell factor receptor c-Kit (CD117); however, the CPC marker SIRPA was expressed in both sphere populations (data on additional surface markers are shown in **Supplementary Fig. 5**). Downregulation of KDR and CD13 is consistent with their being earlier mesodermal markers[28–30], and the absence of CD117 is consistent with cardiac lineage–tracing data[31].

CPC patterning mimics features of heart field development

By regulating FGF and BMP signaling, we generated seven putative CPC sphere populations and isolated them by fluorescence-activated cell sorting (FACS) for gene expression and differentiation analysis (**Fig. 3a**). Inhibition of both signaling pathways enriched the NKX2-5–eGFP$^-$PDPN^{high} (population 1), whereas exposure to BMP4 alone (with FGF signaling inhibited) or BMP4 and bFGF (80 pg/ml or 1 ng/ml) allowed isolation of cells with different NKX2-5–eGFP and PDPN expression: eGFP$^-$PDPN$^+$ (population 2), eGFP$^-$PDPN$^-$ (population 3), eGFP^{low}PDPN$^+$ (population 4), eGFP^{low}PDPN$^-$ (population 5), eGFP$^+$PDPN$^+$ (population 6) and eGFP$^+$PDPN$^-$ (population 7) (**Fig. 3a**,**b**).

Comparison of these cells with earlier MESP1$^+$ mesodermal cells isolated from a *MESP1* reporter derivative of the same hESC line[28] showed much lower expression of *MESP1* in all sphere populations (**Fig. 3c**). *NKX2-5* and *PDPN* expression confirmed expectations based on eGFP levels and sorting and antibody fidelity. The genes

ISL1, *MEF2C*, *SMARCD3* and *TBX5*, encoding cardiac transcriptional regulators, were all upregulated compared to their expression in the MESP1$^+$ cells and were expressed in the NKX2-5–eGFP$^-$PDPN^{high} population before BMP exposure. Whereas expression of the SAN-regulatory genes *TBX3* and *SHOX2* was lower in spheres, *TBX18* was induced, most notably in the NKX2-5–eGFP$^-$PDPN$^+$ populations. Notably, *HCN4*, which *in vivo* in the mouse marks early differentiating FHF CPCs that give rise to primitive left ventricular progenitors[14,16], was induced by BMP4 exposure in this system and remained low in the NKX2-5–eGFP$^-$PDPN^{high} population. These data raise the testable hypothesis that BMP signaling, together with FGF, controls the transition from a multipotent CPC (SHF-like) to a ventricular-specified progenitor (FHF-like). Microarray analysis of five of the populations revealed a large number of genes differentially regulated by BMP4 or bFGF and BMP4, and very close clustering of the subsets positive or negative for PDPN (**Supplementary Fig. 6** and **Supplementary Data Set 1**).

To induce differentiation, we removed dox to turn off *MYC* transgene expression and plated cells in defined endothelial- or cardiomyocyte-promoting conditions. Endothelial induction was

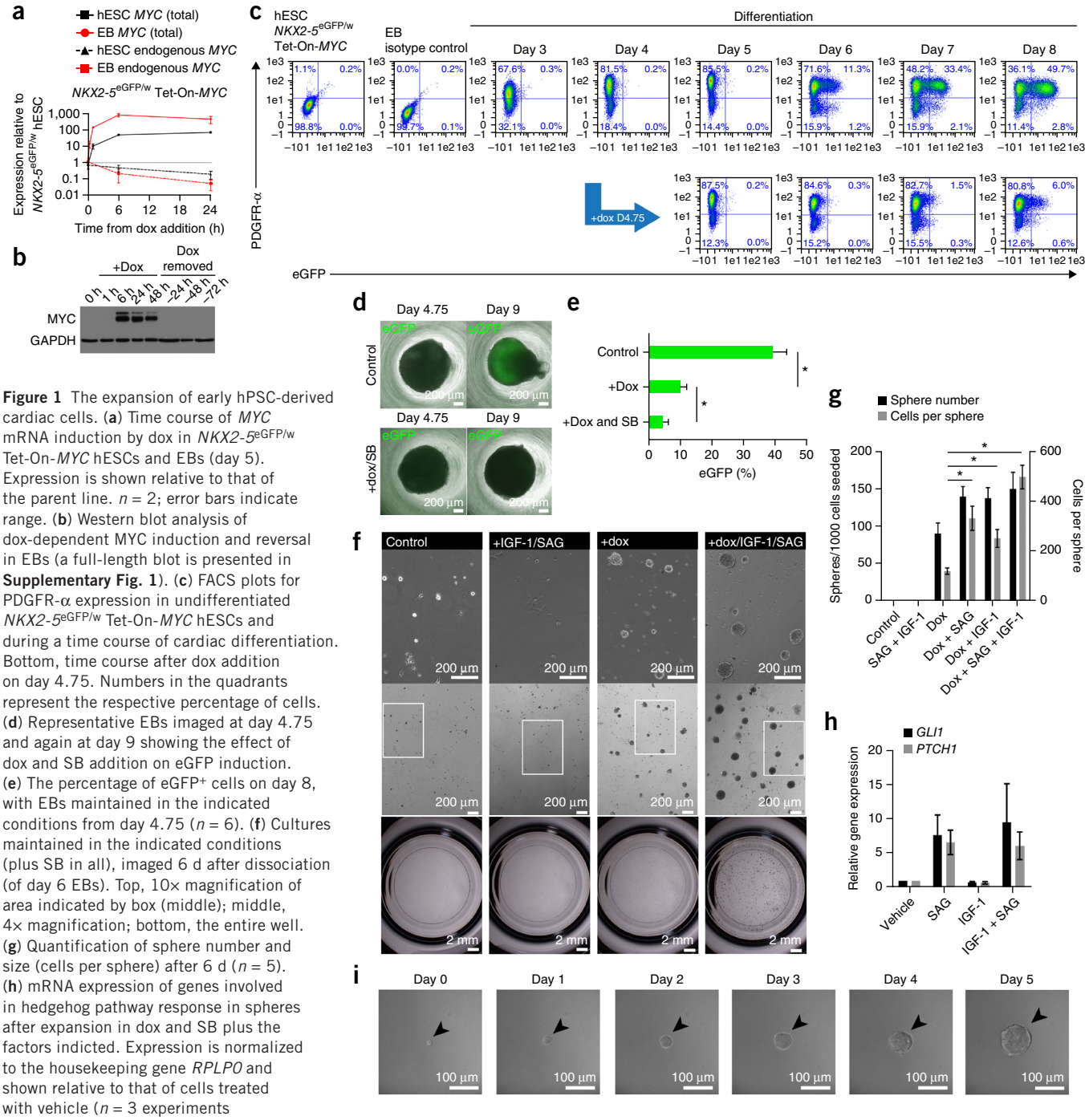

Figure 1 The expansion of early hPSC-derived cardiac cells. (**a**) Time course of *MYC* mRNA induction by dox in *NKX2-5*$^{eGFP/w}$ Tet-On-*MYC* hESCs and EBs (day 5). Expression is shown relative to that of the parent line. $n = 2$; error bars indicate range. (**b**) Western blot analysis of dox-dependent MYC induction and reversal in EBs (a full-length blot is presented in **Supplementary Fig. 1**). (**c**) FACS plots for PDGFR-α expression in undifferentiated *NKX2-5*$^{eGFP/w}$ Tet-On-*MYC* hESCs and during a time course of cardiac differentiation. Bottom, time course after dox addition on day 4.75. Numbers in the quadrants represent the respective percentage of cells. (**d**) Representative EBs imaged at day 4.75 and again at day 9 showing the effect of dox and SB addition on eGFP induction. (**e**) The percentage of eGFP$^+$ cells on day 8, with EBs maintained in the indicated conditions from day 4.75 ($n = 6$). (**f**) Cultures maintained in the indicated conditions (plus SB in all), imaged 6 d after dissociation (of day 6 EBs). Top, 10× magnification of area indicated by box (middle); middle, 4× magnification; bottom, the entire well. (**g**) Quantification of sphere number and size (cells per sphere) after 6 d ($n = 5$). (**h**) mRNA expression of genes involved in hedgehog pathway response in spheres after expansion in dox and SB plus the factors indicted. Expression is normalized to the housekeeping gene *RPLP0* and shown relative to that of cells treated with vehicle ($n = 3$ experiments counting all spheres from 1,000 seeded cells). (**i**) Time-lapse imaging showing a single cell (indicated by arrowheads) proliferating to form a sphere. Error bars in **e**, **g** and **h** indicate s.e.m. *n* signifies independent experiments with independent starting material. $^*P < 0.05$, paired *t*-test.

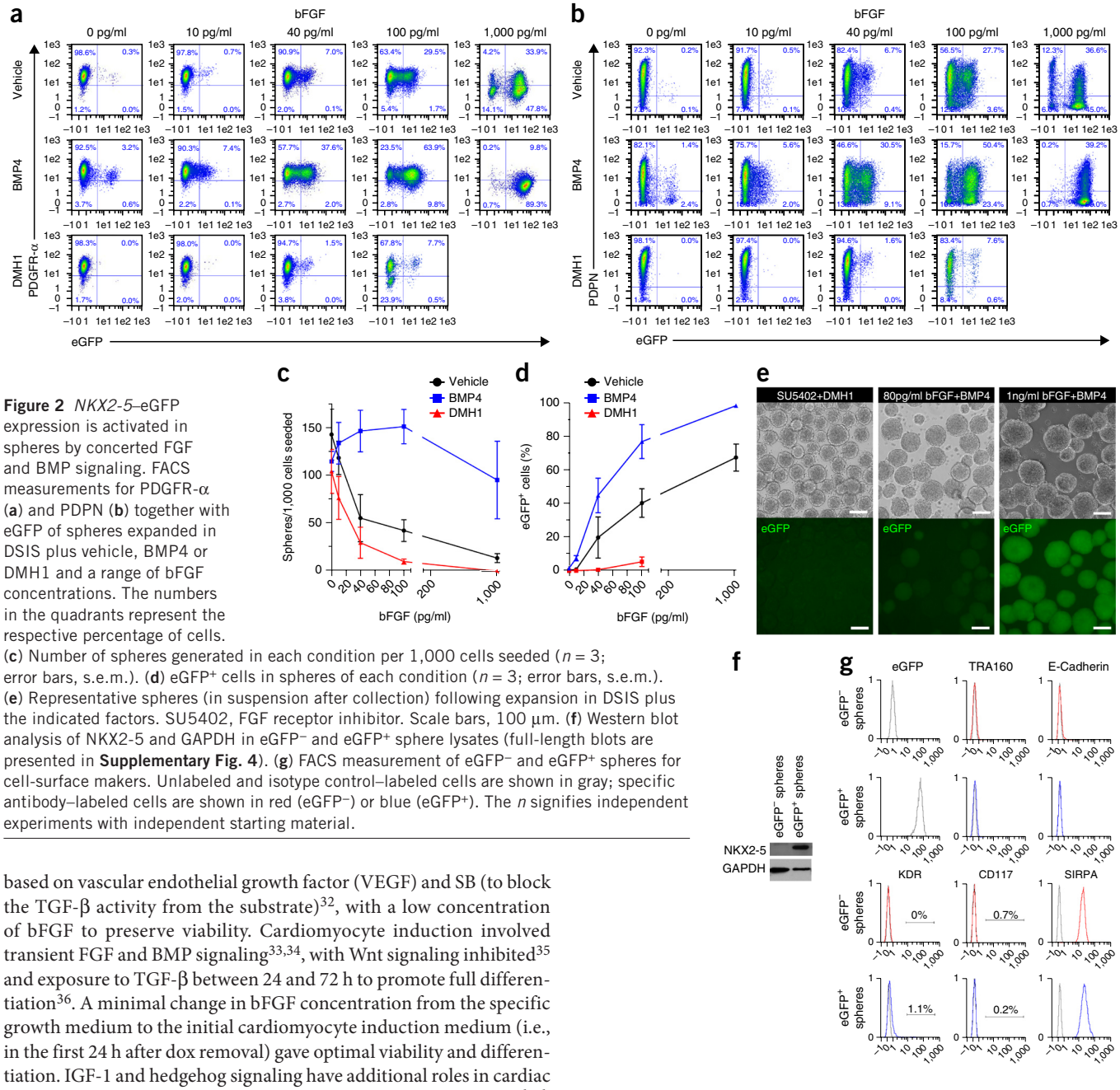

Figure 2 *NKX2-5*–eGFP expression is activated in spheres by concerted FGF and BMP signaling. FACS measurements for PDGFR-α (**a**) and PDPN (**b**) together with eGFP of spheres expanded in DSIS plus vehicle, BMP4 or DMH1 and a range of bFGF concentrations. The numbers in the quadrants represent the respective percentage of cells. (**c**) Number of spheres generated in each condition per 1,000 cells seeded ($n = 3$; error bars, s.e.m.). (**d**) eGFP$^+$ cells in spheres of each condition ($n = 3$; error bars, s.e.m.). (**e**) Representative spheres (in suspension after collection) following expansion in DSIS plus the indicated factors. SU5402, FGF receptor inhibitor. Scale bars, 100 µm. (**f**) Western blot analysis of NKX2-5 and GAPDH in eGFP$^-$ and eGFP$^+$ sphere lysates (full-length blots are presented in **Supplementary Fig. 4**). (**g**) FACS measurement of eGFP$^-$ and eGFP$^+$ spheres for cell-surface makers. Unlabeled and isotype control–labeled cells are shown in gray; specific antibody–labeled cells are shown in red (eGFP$^-$) or blue (eGFP$^+$). The *n* signifies independent experiments with independent starting material.

based on vascular endothelial growth factor (VEGF) and SB (to block the TGF-β activity from the substrate)[32], with a low concentration of bFGF to preserve viability. Cardiomyocyte induction involved transient FGF and BMP signaling[33,34], with Wnt signaling inhibited[35] and exposure to TGF-β between 24 and 72 h to promote full differentiation[36]. A minimal change in bFGF concentration from the specific growth medium to the initial cardiomyocyte induction medium (i.e., in the first 24 h after dox removal) gave optimal viability and differentiation. IGF-1 and hedgehog signaling have additional roles in cardiac differentiation and so were kept active. The NKX2-5–eGFP$^-$PDPN^{high} population gave rise to VE-cadherin$^+$ (VE-cad$^+$) CD31$^+$ endothelial cells with the highest efficiency (46 ± 9%, s.e.m.), whereas eGFP$^+$ cells were much more restricted (**Fig. 3d–f**). The presence of the BMP

Figure 3 Characterization of sphere heterogeneity and differentiation potential. (**a**) Top, schematic showing seven sphere identities and the signaling configuration used to enrich for each. FGF was inhibited with SU5402 (–) or enhanced with 80 pg/ml bFGF (+) or 1 ng/ml bFGF (++); BMP was inhibited with DMH1 or added at a concentration of 20 ng/ml (+). Bottom, FACS plots showing population purity after sorting by eGFP and PDPN. The numbers in the quadrants represent the respective percentage of cells. (**b**) Individual spheres labeled live with anti–PDPN-phycoerythrin (PE) demonstrating the range of clonal identities. (**c**) Gene expression analysis for the sorted sphere populations compared to MESP1$^+$ mesodermal progenitors ($n = 4$). (**d**) FACS measurements of VE-cadherin and eGFP in the same sample after differentiation of sorted populations toward endothelial cells. (**e**) Mean percentage of CD31$^+$ and VE-cadherin$^+$ endothelial cells measured by FACS on differentiation with or without DMH1 ($n = 3$). (**f**) Immunostaining showing typical CD31$^+$/VE-cadherin$^+$ endothelial cells derived from 'Population 1'. (**g**) Live cell images (brightfield and eGFP) after differentiation of sorted populations toward cardiomyocytes. All fields contained substantial areas of contraction (images are from the same fields recorded in **Supplementary Video 2**). (**h**) FACS measurement of population 1 and population 7 for podoplanin (PDPN) and eGFP after differentiation toward cardiomyocytes. (**i,j**) Immunofluorescence for troponin I after cardiomyocyte differentiation of sorted populations. Higher magnification of cardiomyocytes from population 7 is shown (**j**) to highlight the sarcomeric organization. (**k**) Average contraction frequency of beating areas measured 10 d after differentiation ($n = 3$). (**l**) Mean percentage of troponin I$^+$ cells ($n = 3$). Error bars, s.e.m. *n* signifies independent experiments with independent starting material. $^*P < 0.05$, one-way ANOVA with Bonferroni's correction. CM, cardiomyocytes.

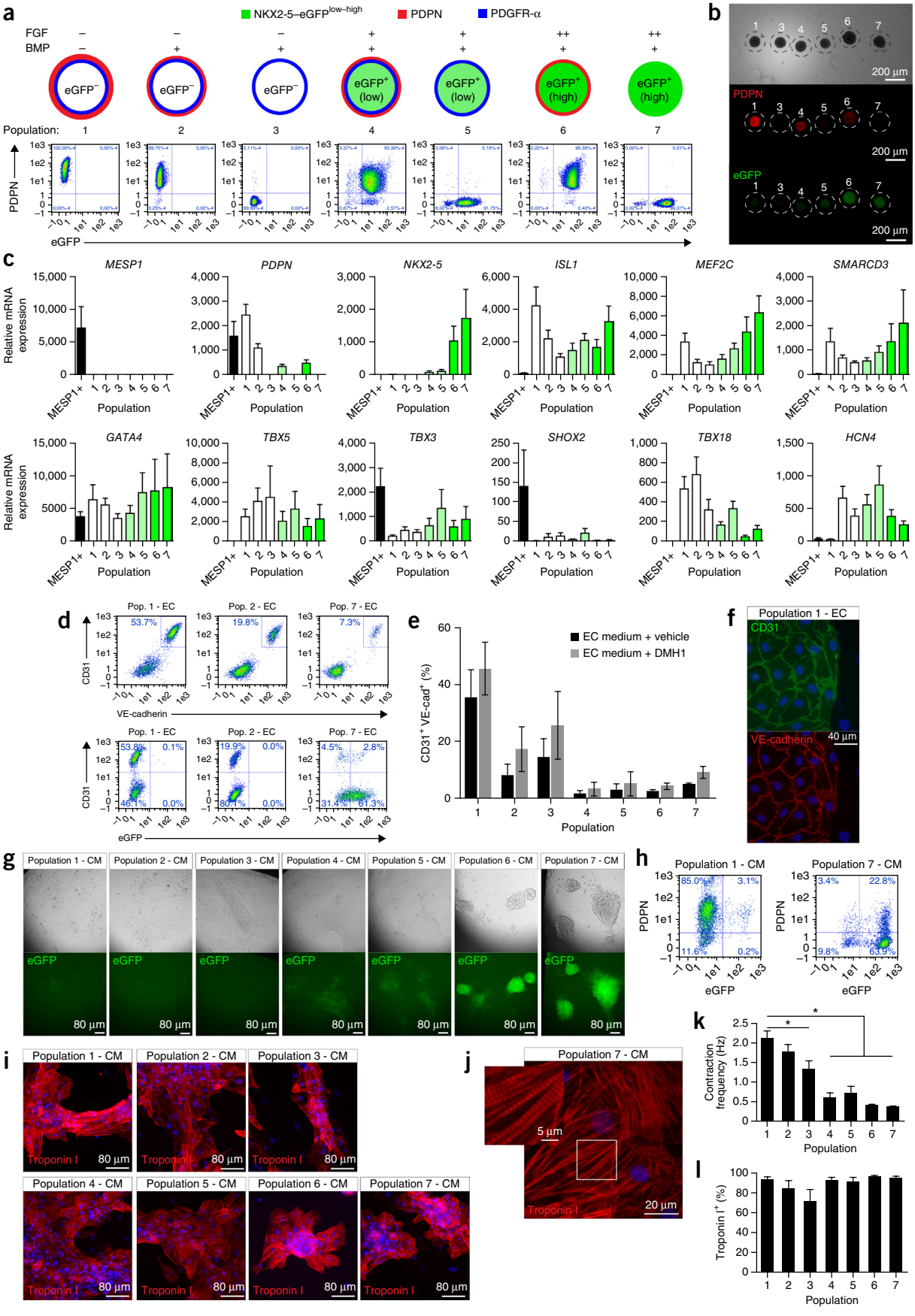

inhibitor DMH1 throughout differentiation improved endothelial differentiation efficiency in every population. In cardiomyocyte-promoting conditions, all populations differentiated with very high efficiency to spontaneously contracting cells. NKX2-5–eGFP expression status was largely maintained on differentiation, with NKX2-5–eGFP⁻ CPCs unexpectedly giving rise primarily to NKX2-5–eGFP⁻ cardiomyocytes (**Fig. 3g–i** and **Supplementary Video 2**). The bFGF and BMP4 present in this window of differentiation as cardiomyocyte-inducing factors were apparently insufficient to induce substantial stable NKX2-5–eGFP expression in these populations. A time-course experiment during differentiation of these CPCs showed that eGFP induction was low (detected in <10% of cells) and mostly transient

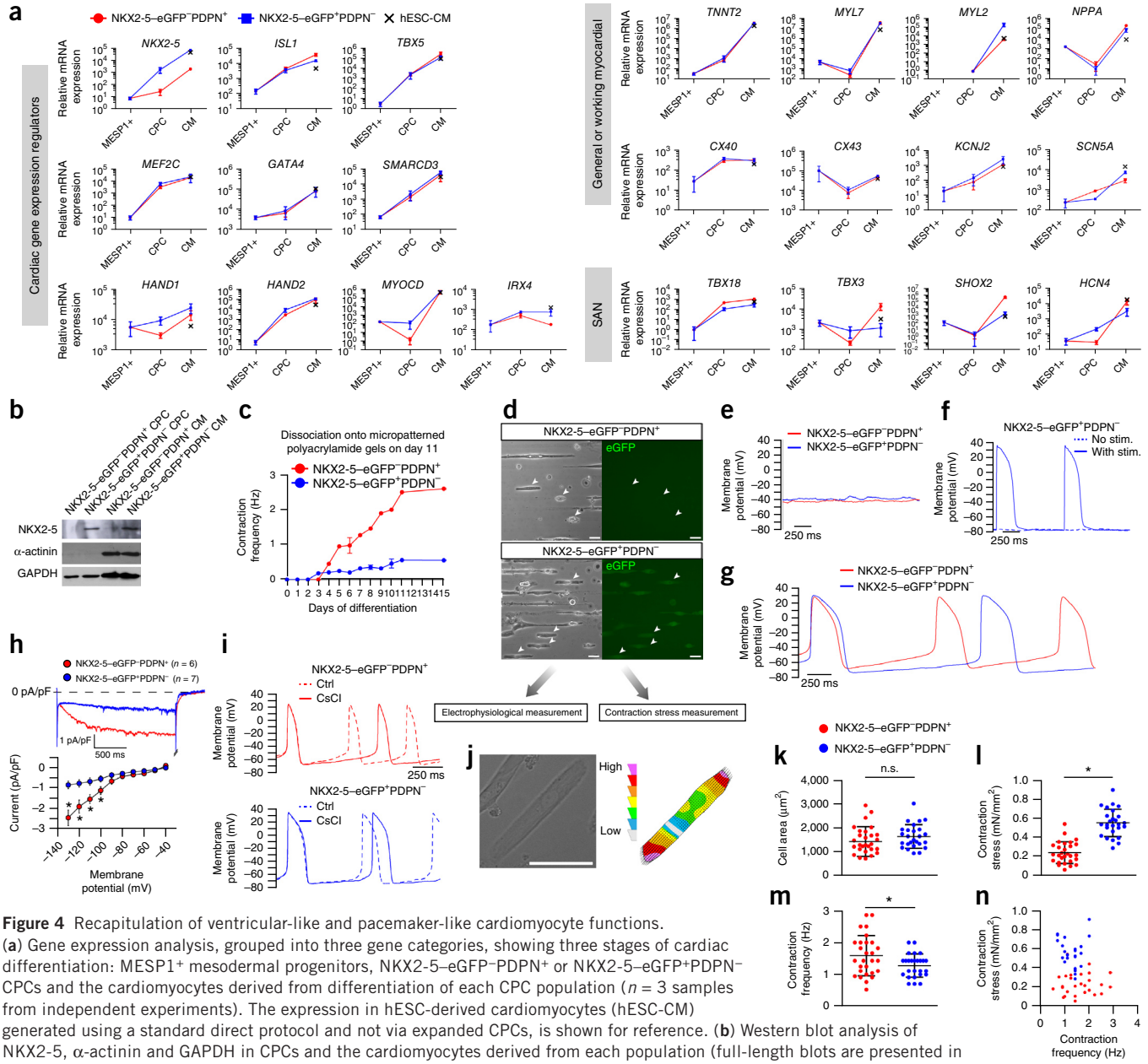

Figure 4 Recapitulation of ventricular-like and pacemaker-like cardiomyocyte functions. (**a**) Gene expression analysis, grouped into three gene categories, showing three stages of cardiac differentiation: MESP1⁺ mesodermal progenitors, NKX2-5–eGFP⁻PDPN⁺ or NKX2-5–eGFP⁺PDPN⁻ CPCs and the cardiomyocytes derived from differentiation of each CPC population ($n = 3$ samples from independent experiments). The expression in hESC-derived cardiomyocytes (hESC-CM) generated using a standard direct protocol and not via expanded CPCs, is shown for reference. (**b**) Western blot analysis of NKX2-5, α-actinin and GAPDH in CPCs and the cardiomyocytes derived from each population (full-length blots are presented in **Supplementary Fig. 9**). (**c**) Contraction frequency measured over time starting from the induction of cardiomyocyte differentiation ($n = 2$ experiments, and each value was an average of duplicate samples). (**d**) Brightfield and eGFP images of typical aligned cells on micropatterned soft polyacrylamide following dissociation of high-density cultures. Contracting cells are indicated with arrows. (**e**) Typical electrophysiological recordings of quiescent cells with a depolarized (>−50 mV) MDP. (**f**) Representative (from 6 measured cells) example of a quiescent NKX2-5–eGFP⁺PDPN⁻ cell with a MDP of around −75 mV without and with suprathreshold stimulation. (**g**) Typical examples of spontaneously active NKX2-5–eGFP⁺PDPN⁻ (from 15 measured cells) and NKX2-5–eGFP⁻PDPN⁺ cells (from 9 measured). (**h**) Typical I_f recordings in response to hyperpolarizing voltage steps from −40 to −130 mV (top) and average current-voltage relationships of I_f (bottom). $n = 6$ NKX2-5⁻ and 7 NKX2-5⁺ cell measurements. $^*P < 0.05$, Mann-Whitney rank sum test. (**i**) Representative examples (from all spontaneous cell measurements) of action potentials in the absence (ctrl) and presence (after 5 min) of 2 mM CsCl. (**j**) Representative contracting cell (from 54 measured cells) and conversion to a vector displacement scale for contraction stress quantification. (**k**) Single-cell surface-area values. (**l**) Single-cell contraction stress values (each representing the peak value from at least 5 contraction cycles). (**m**) Single-cell contraction frequency values (each representing the average frequency over 10 contraction cycles). (**n**) Single-cell contraction stress values plotted against frequency. $^*P < 0.05$, unpaired t-test. n.s., not significant. Error bars, s.e.m. Scale bars, 40 μm (**d**,**j**).

during this exposure period (**Supplementary Fig. 7**), contrasting with the higher sensitivity of proliferating CPCs. On differentiation of populations 6 and 7, NKX2-5–eGFP expression was maintained and became stable and independent of bFGF and BMP4. Apart from derivatives of population 3, all cultures were >80% troponin I$^+$ (**Fig. 3l**). Sarcomeric organization was evident in cardiomyocytes from all populations but was particularly striking in cardiomyocytes from populations 6 and 7 (**Fig. 3j** and **Supplementary Fig. 8**). Contraction frequency was much higher in the cardiomyocyte monolayers from CPC population 1 (**Fig. 3k**). Contractility of these cells also seemed to have more limited dynamic range, contrasting with the lower frequency and more highly dynamic contractility of the NKX2-5–eGFP$^+$ cultures.

Together with the observation of greater potential for endothelial differentiation, these data suggested that the *ISL1*-expressing NKX2-5–eGFP$^-$PDPN^{high} CPCs might resemble primitive SHF-like CPCs and, consequently, be competent for SAN lineage specification.

Table 1 Action potential parameters of single NKX2-5–eGFP$^+$ PDPN$^-$ and NKX2-5–eGFP$^-$PDPN$^+$ cells

	NKX2-5–eGFP$^+$PDPN$^-$ cells		NKX2-5–eGFP$^-$PDPN$^+$ cells
	Stimulated at 1 Hz (n = 6)	Spontaneous (n = 15)	Spontaneous (n = 9)
MDP (mV)	−78.7 ± 1.4†	−74.4 ± 0.7	−68.9 ± 1.9*
dV/dt_{max} (V/s)	44.7 ± 10.6†	16.0 ± 2.7	6.7 ± 1.3*
APA (mV)	105 ± 3†	97 ± 2	84 ± 4*
APD_{20} (ms)	123 ± 16	119 ± 16.9	79 ± 9*
APD_{50} (ms)	179 ± 18	178 ± 12	124±11*
APD_{90} (ms)	207 ± 18	217 ± 13	172 ± 12*
Cycle length (ms)	–	1,330 ± 155	642 ± 108*
DDR_{100} (mV/s)	–	21.6 ± 2.4	37.3 ± 6.2*

Data are mean ± s.e.m.; n, number of cells; DDR_{100}, diastolic depolarization rate over the 100-ms time interval starting at MDP +1 mV. $^\dagger P < 0.05$, stimulated vs. spontaneously active NKX2-5+PDPN$^-$ cells; $^*P < 0.05$, spontaneously active NKX2-5–eGFP$^+$PDPN$^-$ vs. spontaneously active NKX2-5–eGFP$^-$PDPN$^+$ cells (unpaired t-test or Mann-Whitney rank sum test).

CPC differentiation to pacemaker and ventricular myocytes

To better characterize the two most divergent populations, we compared gene expression after cardiomyocyte differentiation of NKX2-5–eGFP$^-$PDPN^{high} and NKX2-5–eGFP$^+$ PDPN$^-$ CPCs, with standard hESC-derived cardiomyocytes from the parental line used as a reference (**Supplementary Table 1**). Sarcomere-related transcripts from *TNNT2* and *MYL7* were induced equally in both populations, consistently with a general cardiomyocyte identity (**Fig. 4a**). Equal α-actinin protein expression was also observed (**Fig. 4b** and **Supplementary Fig. 9**). By contrast, the ventricular marker *MYL2* (encoding MLC2V) was 40-fold higher in the NKX2-5–eGFP$^+$ PDPN$^-$ than in the NKX2-5–eGFP$^-$PDPN$^+$ cardiomyocytes ($P < 0.05$), and *SCN5A*, encoding cardiac sodium channel, was also significantly higher in the same population ($P < 0.05$). The difference in MLC2V expression was confirmed by immunostaining (**Supplementary Fig. 10**). Expression of the genes *TBX5*, *MEF2C*, *GATA4*, *SMARCD3*, *HAND1*, *HAND2* and *MYOCD*, encoding cardiac transcriptional regulators, was increased similarly in each lineage and these genes were also expressed at similar levels in the reference cardiomyocytes. However, consistently with the premise that the NKX2-5–eGFP$^-$PDPN^{high} CPCs tend toward a SAN fate under these conditions, this lineage showed much higher induction of *TBX3* and *SHOX2* (11-fold and 289-fold, respectively) ($P < 0.05$), *TBX18* (3.6-fold) and *HCN4*, the dominant HCN transcript underlying the hyperpolarization-activated current (I_f) in SAN[37] (4.3-fold). Despite these differences, which suggest regional specification, the chamber myocardial marker *NPPA* was induced on differentiation of both populations, and *CX40* and *CX43*, which encode gap junction proteins, were equally expressed. Whether a functional pacemaker phenotype would develop despite seemingly inappropriate expression of such genes requires further validation.

Contracting monolayers of NKX2-5–eGFP$^+$PDPN$^-$ and NKX2-5–eGFP$^-$PDPN$^+$ cardiomyocytes were dissociated to single cells on micropatterned polyacrylamide gels for electrophysiological and contraction stress measurement (**Fig. 4c**,**d**). Spontaneously active and virtually quiescent single cells were subsequently observed in both groups. After electrophysiological analysis, the quiescent cells could be subdivided into those with a depolarized (higher than −50 mV) maximal diastolic potential (MDP) (**Fig. 4e**) or an MDP of approximately −75 mV (**Fig. 4f**). Action potentials (APs) could be elicited by suprathreshold current pulses through the patch pipette in the latter group (**Fig. 4f**) but not in those that were depolarized. Quiescent cells with an MDP of around −75 mV were observed only in the NKX2-5–eGFP$^+$PDPN$^-$ group. **Figure 4g** shows typical examples of spontaneous APs of NKX2-5–eGFP$^+$PDPN$^-$ and NKX2-5–eGFP$^-$PDPN$^+$ cells (average AP parameters are summarized in **Table 1**). AP parameters were notably different between the spontaneously active cells of each group. NKX2-5–eGFP$^-$PDPN$^+$ cells had a higher MDP and a faster diastolic depolarization rate (DDR), which resulted in pacemaker activity with a shorter intrinsic cycle length (CL). Their maximal AP upstroke velocity (dV/dt_{max}) was also lower. In both cell types APs overshot the zero potential value, but the AP amplitude (APA) was lower in NKX2-5–eGFP$^-$PDPN$^+$ cells. APs of NKX2-5–eGFP$^-$ PDPN$^+$ cells repolarized earlier and faster, resulting in shorter AP duration at 20%, 50% and 90% repolarization (APD_{20}, APD_{50} and APD_{90}, respectively). Of note, the stimulated (previously quiescent) NKX2-5–eGFP$^+$PDPN$^-$ cells had a more polarized MDP and higher APA and dV/dt_{max} than did the spontaneously active ones (**Table 1**).

I_f is an important characteristic of pacemaker cells, including those of humans[37]. In NKX2-5–eGFP$^-$PDPN$^+$ cells, I_f density was ~100% higher than in NKX2-5–eGFP$^+$PDPN$^-$ cells ($P < 0.05$) (**Fig. 4h**). In 6 out of the 9 NKX2-5–eGFP$^-$PDPN$^+$ cells and in 7 out of the 15 NKX2-5–eGFP$^+$PDPN$^-$ cells measured under current clamp conditions (**Table 1**), we assessed the contribution of I_f to pacemaker activity. I_f block by CsCl induced a reduction of DDR, as expected, and prolongation of the CL (**Fig. 4i**). The DDR was reduced by an average of 43 ± 7% and 16 ± 7% (s.e.m.), whereas the CL was prolonged by 36 ± 6% and 14 ± 7% in NKX2-5–eGFP$^-$PDPN$^+$ and NKX2-5–eGFP$^+$PDPN$^-$ cells, respectively. The more pronounced decrease in DDR and prolongation of CL in NKX2-5–eGFP$^-$PDPN$^+$ cells is probably due to the higher I_f and HCN4 density in these cells.

Another difference between pacemaker and working myocardial cells is in their contractile force. We measured this using traction force microscopy (**Fig. 4j**). Although spontaneously active NKX2-5–eGFP$^-$PDPN$^+$ and NKX2-5–eGFP$^+$PDPN$^-$ cardiomyocytes were of similar size (**Fig. 4k**), the mean contraction stress was much lower in the NKX2-5–eGFP$^-$ cardiomyocytes ($P < 0.05$) (**Fig. 4l** and **Supplementary Video 3**). The lower contraction stress in the NKX2-5–eGFP$^-$ cardiomyocytes was not due to their higher beating frequency (**Fig. 4m**, $P < 0.05$), as shown by the frequency-contraction stress relationships (**Fig. 4n**). The absence of a positive force-frequency relationship in either population is consistent with previous measurements in PSC-derived cardiomyocytes, which display a fetal level of maturity[38].

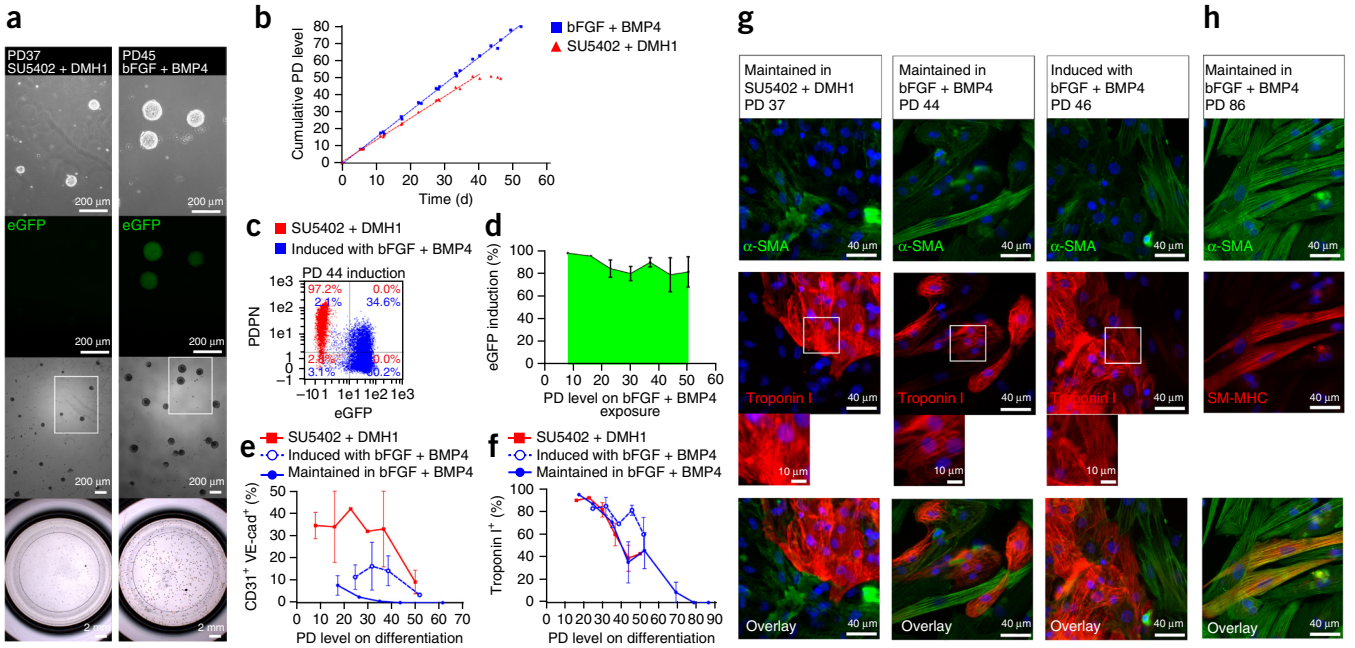

Figure 5 Long-term expansion and differentiation analysis of CPCs. (**a**) CPC spheres expanded for 37 population doublings (PD) in DSIS with SU5402 and DMH1 (eGFP$^-$) or for 45 PD in DSIS + 1 ng/ml bFGF + BMP4 (eGFP$^+$). Images for each condition are of one dish at different magnifications. (**b**) Growth curves of spheres maintained in each culture condition ($n = 3$). (**c**) CPCs expanded to PD 44 in DSIS + SU5402 + DMH1 (red), tested for NKX2-5–eGFP induction capacity by 1 ng/ml bFGF + BMP4 exposure (blue). Each quadrant shows the frequency of each population coded by color. (**d**) NKX2-5–eGFP induction capacity from DSIS + SU5402 + DMH1, measured at progressive population doubling levels ($n = 3$). (**e**) Percentage of CD31$^+$VE-cadherin$^+$ endothelial cells or (**f**) troponin I$^+$ cardiomyocytes generated from each culture condition at progressive population doubling levels (data are from 3 separate CPC expansions). (**g**) Immunofluorescence of α-smooth-muscle actin (α-SMA) and troponin I after cardiomyocyte differentiation of spheres at the indicated doubling level in the condition shown. eGFP fluorescence (in the bFGF + BMP4 conditions) is weak after fixation and does not interfere with interpretation of filament labeling by the α-SMA antibody. (**h**) Immunofluorescence images of α-SMA and smooth muscle myosin heavy chain (SM-MHC) after differentiation of spheres at PD 86. Error bars, s.e.m. *n* signifies independent experiments with independent starting material.

CPCs are clonogenic and possess long-term multipotency

We next tested how frequently clonal lineages of expanded NKX2-5–eGFP$^-$PDPN$^+$ cells retain the capacity to become NKX2-5–eGFP$^+$ as well as self-renew, and whether heterogeneity in differentiation potential existed across this population. Clonal NKX2-5–eGFP$^-$PDPN$^+$ spheres were dissociated into DSIS with SU5402 and DMH1 (self-renewal condition) or DSIS with 1 ng/ml bFGF and BMP4 (*NKX2-5* inducing condition). After 6 d, eGFP was induced in >95% of cells from clones expanded in bFGF and BMP4 and in none of those maintained in the inhibitors, where the NKX2-5–eGFP$^-$PDPN$^+$ status was largely preserved (**Supplementary Fig. 11**). Endothelial differentiation capacity remained stronger in NKX2-5–eGFP$^-$PDPN$^+$ spheres, whereas both populations could generate a high percentage of cardiomyocytes (median troponin I$^+$, ≥90%). Clone-to-clone variation was relatively small, indicating that the initial NKX2-5–eGFP$^-$PDPN$^+$ sphere population may be uniform. The self-renewal of this early SHF-like progenitor population presents an opportunity for applying patterning with retinoic acid to direct CPC specification toward the atrial lineage. The expression profile of cardiomyocytes generated from CPCs exposed to 10 nM retinoic acid prior to differentiation suggested that this response may be present in these cells (**Supplementary Fig. 12**).

To assess the long-term potential of NKX2-5–eGFP$^-$PDPN$^+$ spheres and their NKX2-5–eGFP$^+$ derivative spheres, we expanded the cultures over multiple passages (**Fig. 5a**,**b**). Cells maintained in DSIS with bFGF and BMP4 had a shorter doubling time that did those in DSIS with SU5402 and DMH1 (15.3 h versus 18.6 h, respectively). In three separate experiments the lifespan of NKX2-5–eGFP$^-$PDPN$^+$

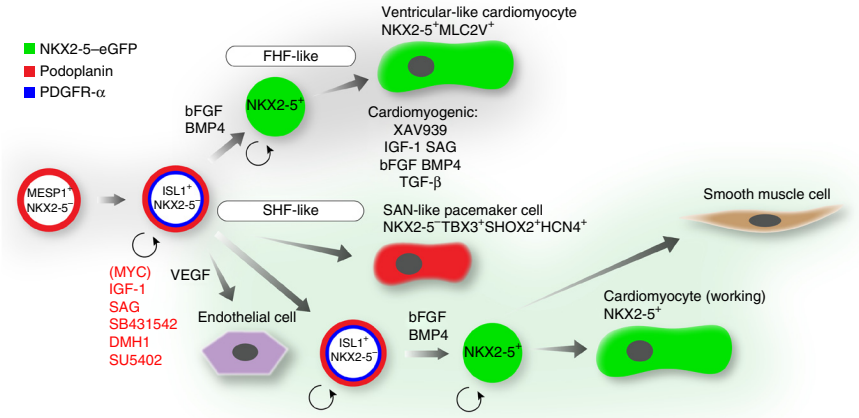

Figure 6 Working model of hPSC-derived cardiovascular progenitor self-renewal and differentiation in the context of heart development.

spheres in DSIS with SU5402 and DMH1 was ~50 population doublings, at which point the cells abruptly stopped growing, whereas cells in DSIS with bFGF and BMP4 grew for >80 doublings without reaching senescence. NKX2-5–eGFP induction capacity was well preserved in NKX2-5–eGFP$^-$PDPN$^+$ CPCs maintained with SU5402 and DMH1, with ~80% of cells, on average, capable of full induction beyond 40 doublings (**Fig. 5c**,**d**). These cells could also generate >30% endothelial cells beyond 35 doublings, whereas CPCs induced to NKX2-5–eGFP$^+$ status were progressively restricted (**Fig. 5e**), as observed above (**Fig. 3e**). Cardiomyocyte differentiation was >80% efficient up to around 30 doublings in all three populations (**Fig. 5f**), beyond which distinctly striated α-SMA$^+$ smooth muscle–like cells (troponin I$^-$) became increasingly prevalent, resulting in more mixed populations (**Fig. 5g**). NKX2-5–eGFP expression was difficult to maintain uniformly beyond 50 doublings (**Supplementary Fig. 13**). Spheres induced over one passage with bFGF and BMP4 gave the highest percentage of cardiomyocytes at higher doubling levels. Beyond 78 doublings, only smooth-muscle cells were generated. The more definitive smooth-muscle marker SM-MHC was also evident in many of these cells (**Fig. 5h**).

DISCUSSION

Studies in developmental biology have provided the foundation for the understanding and control of hPSC differentiation. This has led to effective methods for generating cardiac cell types, but difficulties in maintaining CPCs have hindered specific reconstruction of some aspects of heart development[5]. In this study we developed a system enabling the isolation and robust expansion of pure populations of hPSC-derived CPCs. A central feature of our method is the use of controlled MYC expression to facilitate the maintenance of CPCs. When expressed in a defined time window, MYC arrested CPCs at a pre–NKX2-5$^+$ multipotent stage and acted as an essential permissive element in their continued expansion through IGF-1 and hedgehog signaling. In mouse development, *c-Myc* mRNA is clearly detectable in the embryonic heart and decreases markedly in the neonate[39].

Cardiogenesis is regulated by the tight spatial and temporal control of secreted factors at specific concentrations[40]. Although the early cardiogenic roles of cytokines including BMP, activin and Wnt have been well characterized in the PSC system[17,35,41], control of CPC specification has not be as well studied. The expression of FGF and BMP, particularly by endoderm and ectoderm adjacent to the heart-forming region, is thought to underlie early NKX2-5 expression[22,24–26]. These tissues may have similar inducing roles on the later-differentiating SHF progenitor population, with additional signaling sources being the SHF progenitors themselves and the primary myocardium[7,42]. Here we show that the developmental roles of FGF and BMP are reenacted in hPSC CPCs, and by modulating these signaling pathways we were able to recreate the gene expression signatures of early heart field development (**Fig. 6**) and direct the patterned CPCs toward NKX2-5–eGFP$^-$PDPN$^+$ pacemaker-like myocytes or NKX2-5–eGFP$^+$ ventricular-like working myocytes with appropriate electrophysiological and contractile characteristics. CPC-derived NKX2-5–eGFP$^+$ cardiomyocytes had well-organized sarcomeres and encompassed a population of highly polarized quiescent cells excitable by stimulation—the signature of mature working myocytes. By contrast, the pacemaker-like cells exhibited rapid spontaneous activity owing to their higher I_f. Additionally, we found that NKX2-5–eGFP$^-$PDPN$^+$ CPCs were uniquely susceptible to differentiation to an endothelial fate despite having undetectable levels of KDR expression, which is therefore not essential for this capability. This competence might shed light on the origin of the endocardium[43]. The generation of atrial cardiomyocytes was not the focus of this study, but we showed that retinoic acid may have a role in directing this lineage commitment when applied initially to the self-renewing SHF-like NKX2-5–eGFP$^-$PDPN$^+$ CPCs, consistently with earlier reports[44,45].

CPCs could be expanded to >40 population doublings while retaining multipotent differentiation capacity, a substantial extension compared with previous reports[11,12,29,30,46–51]. Although the use of a *MYC* transgene limits the translational applicability of our approach, the growth stability achieved creates an opportunity to identify factors enabling the expansion of either pre–NKX2-5$^+$ or NKX2-5$^+$ CPCs in the absence of exogenous MYC (i.e., dox-independent growth) or genes that restrain self-renewal, such as those governing cell-cycle arrest mechanisms. This tractable system could be used to help identify the genes conferring CPC potential, and hence the nature of the apparent 'clock' we have observed, which we define as the progressive time-dependent shift in differentiation affinity toward smooth muscle, perhaps in relation to the development of smooth muscle in the heart[52].

We replicated the essential elements of these results in induced hPSCs (**Supplementary Fig. 14** and **Supplementary Video 4**). Such applications could benefit studies aiming to model cardiac disease, for example, by isolating and cryopreserving CPCs, which are later differentiated to the necessary target population. Realizing the potential shown here means that an expansion of more than 10^7-fold from the starting CPC population is feasible. In summary, the identification of MYC as a permissive factor in CPC self-renewal should enable the use of expandable PSC-derived CPCs for a variety of applications relating to modeling or regenerating the human heart.

METHODS

Methods and any associated references are available in the online version of the paper.

Note: Any Supplementary Information and Source Data files are available in the online version of the paper.

ACKNOWLEDGMENTS

We acknowledge the contributions of I. Marcuccio and S. Casini. Work in C.L.M.'s lab is supported by Cardiovascular Research Netherlands (CVON HUSTCARE), The Netherlands Institute of Regenerative Medicine (NIRM), the European Research Council (ERCAdG 323182 STEMCARDIOVASC) and The Netherlands Organization for Scientific Research (NWO-FOM FOM 09MMC02). Work in R.P.'s lab is supported by the Netherlands Organization for Scientific Research (ZonMW-TOP 40-00812-98-12086 and ZonMW-MKMD 40-42600-98-036) and the Rembrandt Institute of Cardiovascular Science. V.V.O. was supported by the European Community's Seventh Framework Programme (FP7/2007-2013) grant agreement 602423.

AUTHOR CONTRIBUTIONS

M.J.B. and C.L.M. designed the study. M.J.B., M.C.R., A.O.V., A.R.L. and V.S. performed experiments and analyzed data. H.D.D. analyzed data. M.J.B., C.L.M. and A.O.V. wrote the manuscript. D.W. maintained and differentiated the PSCs. S.C.d.H. generated and provided the *MESP1*$^+$ RNA. M.B. generated and provided the original hPSC lines. V.V.O. helped with experimental design. R.P. and C.L.M. supervised the study. All authors edited the manuscript.

COMPETING FINANCIAL INTERESTS

The authors declare no competing financial interests.

1. Drawnel, F.M. *et al.* Disease modeling and phenotypic drug screening for diabetic cardiomyopathy using human induced pluripotent stem cells. *Cell Reports* **9**, 810–820 (2014).
2. Matsa, E., Burridge, P.W. & Wu, J.C. Human stem cells for modeling heart disease and for drug discovery. *Sci. Transl. Med.* **6**, 239ps6 (2014).

3. Lundy, S.D., Gantz, J.A., Pagan, C.M., Filice, D. & Laflamme, M.A. Pluripotent stem cell derived cardiomyocytes for cardiac repair. *Curr. Treat. Options Cardiovasc. Med.* **16**, 319 (2014).
4. Bhave, M., Akhter, N. & Rosen, S.T. Cardiovascular toxicity of biologic agents for cancer therapy. *Oncology* **28**, 482–490 (2014).
5. Birket, M.J. & Mummery, C.L. Pluripotent stem cell derived cardiovascular progenitors—a developmental perspective. *Dev. Biol.* **400**, 169–179 (2015).
6. Vincent, S.D. & Buckingham, M.E. How to make a heart: the origin and regulation of cardiac progenitor cells. *Curr. Top. Dev. Biol.* **90**, 1–41 (2010).
7. Cai, C.-L. *et al.* Isl1 identifies a cardiac progenitor population that proliferates prior to differentiation and contributes a majority of cells to the heart. *Dev. Cell* **5**, 877–889 (2003).
8. Lints, T.J., Parsons, L.M., Hartley, L., Lyons, I. & Harvey, R.P. Nkx-2.5: a novel murine homeobox gene expressed in early heart progenitor cells and their myogenic descendants. *Development* **119**, 419–431 (1993).
9. Ma, Q., Zhou, B. & Pu, W.T. Reassessment of Isl1 and Nkx2–5 cardiac fate maps using a Gata4-based reporter of Cre activity. *Dev. Biol.* **323**, 98–104 (2008).
10. Laugwitz, K.-L. *et al.* Postnatal isl1^{+} cardioblasts enter fully differentiated cardiomyocyte lineages. *Nature* **433**, 647–653 (2005).
11. Moretti, A. *et al.* Multipotent embryonic isl1^{+} progenitor cells lead to cardiac, smooth muscle, and endothelial cell diversification. *Cell* **127**, 1151–1165 (2006).
12. Wu, S.M. *et al.* Developmental origin of a bipotential myocardial and smooth muscle cell precursor in the mammalian heart. *Cell* **127**, 1137–1150 (2006).
13. Mommersteeg, M.T.M. *et al.* Molecular pathway for the localized formation of the sinoatrial node. *Circ. Res.* **100**, 354–362 (2007).
14. Wiese, C. *et al. Circ. Res.* **104**, 388–397 (2009).
15. Liang, X. *et al.* HCN4 dynamically marks the first heart field and conduction system precursors. *Circ. Res.* **113**, 399–407 (2013).
16. Später, D. *et al.* A HCN4^{+} cardiomyogenic progenitor derived from the first heart field and human pluripotent stem cells. *Nat. Cell Biol.* **15**, 1098–1106 (2013).
17. Kattman, S.J. *et al.* Stage-specific optimization of activin/nodal and BMP signaling promotes cardiac differentiation of mouse and human pluripotent stem cell lines. *Cell Stem Cell* **8**, 228–240 (2011).
18. Wierstra, I. & Alves, J. The *c-myc* promoter: still mysterY and challenge. *Adv. Cancer Res.* **99**, 113–333 (2008).
19. Gittenberger-De Groot, A.C. *et al.* Nkx2.5 negative myocardium of the posterior heart field and its correlation with podoplanin expression in cells from the developing cardiac pacemaking and conduction system. *Anat. Rec.* **290**, 115–122 (2007).
20. Dyer, L.A. *et al.* BMP signaling modulates hedgehog-induced secondary heart field proliferation. *Dev. Biol.* **348**, 167–176 (2010).
21. Gude, N. *et al.* Akt promotes increased cardiomyocyte cycling and expansion of the cardiac progenitor cell population. *Circ. Res.* **99**, 381–388 (2006).
22. Keren-Politansky, A., Keren, A. & Bengal, E. Neural ectoderm-secreted FGF initiates the expression of Nkx2.5 in cardiac progenitors via a p38 MAPK/CREB pathway. *Dev. Biol.* **335**, 374–384 (2009).
23. Liberatore, C.M., Searcy-Schrick, R.D., Vincent, E.B. & Yutzey, K.E. *Nkx-2.5* gene induction in mice is mediated by a Smad consensus regulatory region. *Dev. Biol.* **244**, 243–256 (2002).
24. Reifers, F., Walsh, E.C., Leger, S., Stainier, D.Y. & Brand, M. Induction and differentiation of the zebrafish heart requires fibroblast growth factor 8 (fgf8/acerebellar). *Development* **127**, 225–235 (2000).
25. Schultheiss, T.M., Burch, J.B. & Lassar, A.B. A role for bone morphogenetic proteins in the induction of cardiac myogenesis. *Genes Dev.* **11**, 451–462 (1997).
26. Barron, M., Gao, M. & Lough, J. Requirement for BMP and FGF signaling during cardiogenic induction in non-precardiac mesoderm is specific, transient, and cooperative. *Dev. Dyn.* **218**, 383–393 (2000).
27. Inman, G.J. *et al.* SB-431542 is a potent and specific inhibitor of transforming growth factor-β superfamily type I activin receptor-like kinase (ALK) receptors ALK4, ALK5, and ALK7. *Mol. Pharmacol.* **62**, 65–74 (2002).
28. Den Hartogh, S.C. *et al.* Dual reporter *MESP1*$^{mCherry/w}$-*NKX2–5*$^{eGFP/w}$ hESCs enable studying early human cardiac differentiation. *Stem Cells* **33**, 56–67 (2015).
29. Yang, L. *et al.* Human cardiovascular progenitor cells develop from a KDR^{+} embryonic-stem-cell-derived population. *Nature* **453**, 524–528 (2008).
30. Ardehali, R. *et al.* Prospective isolation of human embryonic stem cell-derived cardiovascular progenitors that integrate into human fetal heart tissue. *Proc. Natl. Acad. Sci. USA* **110**, 3405–3410 (2013).
31. van Berlo, J.H. *et al.* c-kit^{+} cells minimally contribute cardiomyocytes to the heart. *Nature* **509**, 337–341 (2014).
32. James, D. *et al.* Expansion and maintenance of human embryonic stem cell-derived endothelial cells by TGFβ inhibition is Id1 dependent. *Nat. Biotechnol.* **28**, 161–166 (2010).
33. Marques, S.R., Lee, Y., Poss, K.D. & Yelon, D. Reiterative roles for FGF signaling in the establishment of size and proportion of the zebrafish heart. *Dev. Biol.* **321**, 397–406 (2008).
34. de Pater, E. *et al.* Bmp signaling exerts opposite effects on cardiac differentiation. *Circ. Res.* **110**, 578–587 (2012).
35. Ueno, S. *et al.* Biphasic role for Wnt/β-catenin signaling in cardiac specification in zebrafish and embryonic stem cells. *Proc. Natl. Acad. Sci. USA* **104**, 9685–9690 (2007).
36. Goumans, M.-J. *et al.* TGF-β1 induces efficient differentiation of human cardiomyocyte progenitor cells into functional cardiomyocytes *in vitro*. *Stem Cell Res.* **1**, 138–149 (2007).
37. Verkerk, A.O., van Ginneken, A.C.G. & Wilders, R. Pacemaker activity of the human sinoatrial node: role of the hyperpolarization-activated current, I(f). *Int. J. Cardiol.* **132**, 318–336 (2009).
38. Xi, J. *et al.* Comparison of contractile behavior of native murine ventricular tissue and cardiomyocytes derived from embryonic or induced pluripotent stem cells. *FASEB J.* **24**, 2739–2751 (2010).
39. Jackson, T. *et al.* The c-myc proto-oncogene regulates cardiac development in transgenic mice. *Mol. Cell. Biol.* **10**, 3709–3716 (1990).
40. Noseda, M., Peterkin, T., Simões, F.C., Patient, R. & Schneider, M.D. Cardiopoietic factors extracellular signals for cardiac lineage commitment. *Circ. Res.* **108**, 129–152 (2011).
41. Cai, W. *et al.* Coordinate Nodal and BMP inhibition directs Baf60c-dependent cardiomyocyte commitment. *Genes Dev.* **27**, 2332–2344 (2013).
42. Waldo, K.L. *et al.* Conotruncal myocardium arises from a secondary heart field. *Development* **128**, 3179–3188 (2001).
43. Milgrom-Hoffman, M. *et al.* The heart endocardium is derived from vascular endothelial progenitors. *Development* **138**, 4777–4787 (2011).
44. Zhang, Q. *et al.* Direct differentiation of atrial and ventricular myocytes from human embryonic stem cells by alternating retinoid signals. *Cell Res.* **21**, 579–587 (2011).
45. Devalla, H.D. *et al.* Atrial-like cardiomyocytes from human pluripotent stem cells are a robust preclinical model for assessing atrial-selective pharmacology. *EMBO Mol. Med.* **7**, 394–410 (2015).
46. Kattman, S.J., Huber, T.L. & Keller, G.M. Multipotent Flk-1^{+} cardiovascular progenitor cells give rise to the cardiomyocyte, endothelial, and vascular smooth muscle lineages. *Dev. Cell* **11**, 723–732 (2006).
47. Qyang, Y. *et al.* The renewal and differentiation of Isl1^{+} cardiovascular progenitors are controlled by a WNT/β-catenin pathway. *Cell Stem Cell* **1**, 165–179 (2007).
48. Bu, L. *et al.* Human ISL1 heart progenitors generate diverse multipotent cardiovascular cell lineages. *Nature* **460**, 113–117 (2009).
49. Domian, I.J. *et al.* Generation of functional ventricular heart muscle from mouse ventricular progenitor cells. *Science* **326**, 426–429 (2009).
50. Moretti, A. *et al.* Mouse and human induced pluripotent stem cells as a source for multipotent Isl1^{+} cardiovascular progenitors. *FASEB J.* **24**, 700–711 (2010).
51. Elliott, D.A. *et al. NKX2–5*$^{eGFP/w}$ hESCs for isolation of human cardiac progenitors and cardiomyocytes. *Nat. Methods* **8**, 1037–1040 (2011).
52. Miano, J.M., Cserjesi, P., Ligon, K.L., Periasamy, M. & Olson, E.N. Smooth muscle myosin heavy chain exclusively marks the smooth muscle lineage during mouse embryogenesis. *Circ. Res.* **75**, 803–812 (1994).

ONLINE METHODS

Tet-On-*MYC* hPSC line generation and maintenance. NKX2-5$^{eGFP/w}$ hESCs generated previously[51] and hiPSCs generated previously (LQT2-hiPSCs^{N996I} and LQT2-hiPSCs^{Corr})[53] were maintained on mouse embryonic fibroblasts in DMEM/F12-based medium containing 20% knockout serum replacement (Invitrogen) and 10 ng/ml bFGF (Miltenyi Biotech). hPSCs were passaged using TrypLE Select (Invitrogen). A Tet-On-*MYC* system was introduced into each line by transducing the hPSCs with two lentiviruses, one carrying a *MYC T58A* transgene under the control of a TRE-CMV promoter (Addgene plasmid #19775), and the second carrying the tetracycline transactivator (Addgene plasmid #19780)[54]. Titers giving transduction efficiencies of approximately 40% (based on a GFP expressing control lentivirus) were used to avoid multiple viral insertions. Clones were isolated following single-cell FACS deposition and selected for their ability to efficiently upregulate *MYC* on exposure to 1 μg/ml doxycycline (Sigma-Aldrich). The lines used had normal karyotypes and were negative for mycoplasma contamination.

hPSC differentiation. Differentiations were performed in serum-free BPEL medium containing 1 μg/ml insulin using an embryoid body (EB) system as previously described[55]. The following growth factors were present for the first 3 d of differentiation: 30 ng/ml BMP4 (R&D), 20 ng/ml Activin A (Miltenyi Biotech), 30 ng/ml VEGF (Miltenyi Biotech), 40 ng/ml SCF (Miltenyi Biotech) and 1.5 μM CHIR99021 (Axon Medchem). On day 4.75, control wells were refreshed again with BPEL medium with or without vehicle, or for *MYC* induction with medium containing 1 μg/ml doxycycline ± 5 μM SB431542 (Tocris Bioscience). EBs were maintained in these conditions for subsequent FACS, RNA or protein analysis or dissociated on day 6 for progenitor expansion.

CPC culture maintenance and differentiation. CPCs were seeded on a thin layer of undiluted Matrigel (14 μl/cm^2) (growth factor reduced; Corning 354230) in organ culture dishes (BD Falcon) in BPEL medium containing 5 μM SB431542 with or without the following experimental factors: 1 μg/ml doxycycline, 100 ng/ml LONG R3 IGF-1 (hereafter, IGF-1), 1 μM SAG (Millipore), 0.5 μM DMH1 (ref. 56), 10 μM SU5402, 10–1,000 pg/ml bFGF (Miltenyi Biotech), 20 ng/ml BMP4 (R&D). Reagents were obtained from Sigma-Aldrich unless stated otherwise. Cultures were refreshed every 2 d. Growing cell spheres were manually collected after 6 d under a dissecting microscope, dissociated using TrypLE Select and either plated for differentiation or replated on fresh Matrigel at a density of 350–1,700 cells/cm^2 depending on the condition. Long-term expansions were carried out at 3% O_2 to minimize cellular senescence. For clonal analysis, single cell deposition of eGFP$^-$PDPN$^+$ cells into Matrigel-coated 96-well plates was performed by FACS from EBs at day 6 of differentiation. Clonal spheres were picked 6 d later for propagation.

Cardiomyocyte differentiation was induced by plating cells at a density of 10^5 cells per cm^2 on Matrigel-coated (1:100 dilution) 96-well plates (BD Falcon) in BPEL medium supplemented with 100 ng/ml IGF-1, 1 μM SAG, 1 μM XAV 939 (Tocris Bioscience), 100 or 1,000 pg/ml bFGF (for NKX2-5–eGFP$^-$ and NKX2-5–eGFP$^+$ CPCs, respectively) and 20 ng/ml BMP4. From 24–72 h of differentiation cells were all in the BPEL medium supplemented with 100 ng/ml IGF-1, 1 μM SAG, 1 μM XAV 939, 100 pg/ml bFGF and 2.5 ng/ml TGF-β1 (Peprotech). At 72 h the medium was changed to BPEL supplemented with 100 ng/ml IGF-1, 1 μM XAV 939 and 10 pg/ml bFGF. At 96 h onward the beating cardiomyocytes were maintained in contractility-promoting medium (unpublished data) containing 100 ng/ml IGF-1, 30 μM 3,3′,5-triiodo-L-thyronine sodium salt (T3) and 1 μM dexamethasone (Sigma-Aldrich).

Endothelial differentiation was induced by plating cells at a density of 0.6 × 10^5 cells/cm^2 on Matrigel-coated 96-well plates (BD Falcon) in BPEL medium supplemented with 100 ng/ml IGF-1, 50 ng/ml VEGF, 50 pg/ml bFGF, 5 μM SB431542 and 0.5 μM DMH1. Medium was refreshed at 48 h. At 96 h DMH1 was removed. Cells were analyzed by FACS or fixed after a further 2 d.

Flow cytometry and cell sorting. Staining was done in PBS containing 1 mM EDTA and 0.5% BSA. The antibodies and dilutions used were as follows: anti-PDGFRα-BV421 (BD Bioscience cat no. 562799; 1:50), anti-podoplanin-PE (eBioscience cat no. 12-9381-41; 1:500), anti-VEGFR2-PE (R&D cat no. FAB357P; 1:50), anti-VEGFR3-PE (R&D cat no. FAB3492P; 1:50), anti-VE-cadherin-PE (eBioscience cat no. 12-1449-80; 1:150), anti-CD31-APC (eBioscience cat no. 17-0319-42; 1:150), anti-CD90-PE (BD cat no. 555596; 1:500), anti-CD146-PE (BD cat no. 550315; 1:20), anti-NG2-PE (R&D cat no. FAB2585P; 1:20), anti-PDGFRβ-PE (BD cat no. 558821; 1:20), anti-E-cadherin-APC (R&D cat no. FAB18381A; 1:40), anti-TRA-1-60-PE (Miltenyi Biotec cat no. 130-100-347; 1:100), anti-CD73-PE (BD cat no. 550257; 1:20), anti-CD105-PE (Life Technologies cat no. MHCD10504; 1:20), anti-CD13-BV421 (BioLegend cat no. 301716; 1:50), anti-CKIT-APC (BD Bioscience cat no. 550412; 1:100), anti-SIRPα (Biolegend cat no. 323801; 1:500, or Miltenyi Biotec 130-099-793; 1:50), PE anti-mouse IgG (Jackson Immuno Research cat no: 115-116-146; 1:200), mouse IgG2a-BV421 isotype control (BD Bioscience cat no. 562439), mouse IgG1-PE isotype control (Miltenyi Biotec 130-098-845), mouse IgG2b-APC isotype control (R&D cat no. IC0041A). Samples were measured with a MACSQuant VYB (Miltenyi Biotech) equipped with a violet (405 nm), blue (488 nm) and yellow (561 nm) laser. Cell sorting was performed on a BD FACSAria III (BD Bioscience).

Immunostaining and microscopy. Cells were fixed with 2% paraformaldehyde or methanol (for MLC2V) and permeabilized with 0.1% Triton X-100. Blocking was achieved with 4% normal goat serum. Primary antibody incubations were overnight in 4% normal goat serum at 4 °C using the following antibodies: anti-troponin I (clone H170, Santa Cruz; 1:500), anti-MLC2V (Synaptic Systems 310 111; 1:50), anti-α-smooth muscle actin (Sigma A2547; 1:300), anti-myosin (smooth muscle) heavy chain (Biomedical Technologies BT-562; 1:200), anti-VE-cadherin (Cell Signaling; 1:200) and anti-CD31 (DAKO M0823; 1:20). Secondary antibodies were Alexa 488 anti-mouse and Alexa 555 anti-rabbit (Invitrogen). eGFP fluorescence was reduced to background levels after fixation and could be differentiated from the specific smooth muscle type-α–smooth muscle actin staining. Nuclei were labeled with DAPI.

Quantitative real time PCR. RNA was isolated using a Minelute RNA extraction kit (Qiagen) and cDNA synthesized using an iScript cDNA synthesis kit (BioRad). Real-time PCR was performed on a Bio-Rad CFX96 machine using IQ SYBR Green (Bio-Rad). Gene expression values were normalized to the mean expression of the housekeeping genes encoding a human ribosomal protein (*RPLP0*), glucuronidase (*GUSB*), and *RNF7*. RNA from *MESP1*-expressing sorted cells was obtained from a derivative knock-in reporter line and used as a reference[28]. The hESC-cardiomyocyte control RNA was obtained from eGFP$^+$ sorted cells from a standard monolayer differentiation of the *NKX2-5*$^{eGFP/w}$ hESC line with maintenance in the same medium as the CPC-CMs. Expression of *NKX2-5* is presented as an average of mRNA from both alleles.

Primer sequences are shown in **Supplementary Table 2**.

Whole genome arrays and data analysis. Gene expression was determined on the HumanHT-12 v4 Expression BeadChip at ServiceXS, Leiden, The Netherlands. RNA was isolated from FACS sorted cells using a NucleoSpin RNA extraction kit (Macherey-Nagel). Biotin-labeled cRNA samples were amplified with Illumina TotalPrepTM-96 RNA Amplification Kit. Hybridization and scanning were performed according to standard Illumina protocols. Expression profiles were established for CPC 'Populations 1, 2, 3, 6 and 7' on the basis of duplicate samples collected from independent differentiations. Data were analyzed using GeneSpring v13.0 (Agilent Technologies) using the percentile shift method of normalization. Statistical significance was determined with one-way ANOVA test and multiple testing corrections were performed using Benjamini-Hochberg test. $P < 0.05$ was considered significant. All samples were compared against 'Population 1' and differentially expressed genes were identified with a fold change cut-off of >2.0.

Immunoblotting. Samples were lysed with ice cold ELB (50 mM HEPES (pH 7.0); 250 mM NaCl; 5 mM EDTA; 0.1% NP-40) or RIPA (25 mM Tris-HCl (pH 7.6); 150 mM NaCl; 1% Triton X-100; 0.1% SDS; 1% sodium deoxycholate) with 1:100 Protease Inhibitor Cocktail (Sigma-Aldrich) for 30 min on ice. The samples were centrifuged at 7,000 × *g* for 10 min, and the supernatant was quantified for protein content (Bradford dye-binding method). 30 μg of sample was run in a 10% polyacrylamide gel together with the protein ladder (Precision Plus Protein dual color, Bio-Rad). Proteins were transferred to an Amersham Hybond membrane (GE Healthcare Life Sciences) overnight.

doi:10.1038/nbt.3271

Membranes were blocked with 2% milk in PBS. Membranes were probed with the following: rabbit IgG anti-MYC (Cell Signaling 5605S; 1:1,000), goat IgG anti-NKX2-5 (Santa Cruz SC8697; 1:500), mouse IgG anti–α-actinin (Sigma A7811), or a rabbit IgG anti-GAPDH (Abcam AB9485; 1:2,000) as a loading control. Primary antibodies were detected with the following: anti-rabbit IgG–HRP (Cell Signaling 7074S), anti-mouse IgG–HRP (Cell Signaling 7076) or anti-goat IgG–HRP (Jackson Laboratories).

Patterned polyacrylamide gel fabrication. Patterned polyacrylamide gels were prepared as previously described[57]. Briefly, a 1% gelatin solution was activated with 3.5 mg/mL sodium periodate (Sigma-Aldrich). A polydimethylsiloxane (PDMS) stamp was cast from a SU8 master produced by standard soft lithography techniques and incubated with the activated 1% gelatin solution for 45 min. The excess of gelatin was removed with a nitrogen gun and the stamp was used to micro-contact (μcontact) print a pattern of 20-μm thick with 20-μm spacing gelatin lines onto 10-mm (electrophysiology) or 15-mm (contraction assay) coverslips. The polyacrylamide solution was prepared with a final concentration of 0.1% bisacrylamide (Bio-Rad), 5% acrylamide (Bio-Rad) and 10 mM HEPES (pH 8.5) in distilled water, followed by centrifugation for 1 min at 10,000 r.p.m. for degassing. 0.006% (m/v) of ammonium persulfate (Sigma-Aldrich) and a 1:1,000 dilution of 0.2-μm fluorescent beads (excitation/emission 660/680 nm; Molecular Probes) were added to the solution (for the contraction assay) and briefly vortexed. The gel polymerization was initiated with TEMED (Bio-Rad) and 4.08 μl or 9.2 μl of the final solution was added to a 15 mm or 25 mm coverslip treated with plus Bind-Silane solution (GE Healthcare). The μcontact-printed coverslip was applied on top of the drop with the gelatin lines facing the gel. After 20 min of polymerization, the 10 mm or 15 mm coverslip was removed. Each 25-mm coverslip was mounted in the well of a glass-bottom 6-well plate (Mattek). The 15-mm coverslips were placed in normal tissue culture plates and 10 mm borosilicate rings (Corning) were placed on top of each gel to aid cell seeding. Plates were UV-sterilized and rehydrated with culture medium for 30 min before use. The polymerized gel has a Young's modulus of 5.8 kPa.

Contraction force measurements. Contraction force measurements were performed in normal culture medium in an environment maintained at 37 °C with 5% CO_2. Briefly, using a Leica AF-6000LX microscope, an image-series of aligned single spontaneously contracting cardiomyocytes was taken at 40× magnification at 20 frames per second, recording brightfield and fluorescent beads. Single frames from maximal relaxation and contraction of the brightfield and fluorescent beads image-series were analyzed by the LIBTRC software package (provided by M. Dembo), creating a mask of the cell outline from the brightfield image and a vector map from the difference between the relaxed and contracted fluorescent beads images. The vector map and the cell mask were used to calculate the total force that the cell applies on the substrate at its maximum peak of contraction. The contraction stress generated by the cardiomyocyte during contraction was calculated by dividing the total force by the cell surface area.

Cellular electrophysiology. *Recording procedures.* APs and I_f were recorded at 36 ± 0.2 °C in single cells by the amphotericin-perforated patch-clamp technique using an Axopatch 200B amplifier (Molecular Devices, USA) 5–7 d after dissociation on day 11 of differentiation. Cells were superfused with Tyrode's solution containing (in mM): NaCl 140; KCl 5.4; $CaCl_2$ 1.8; $MgCl_2$ 1.0; glucose 5.5; and HEPES 5.0 (pH 7.4; NaOH). Patch pipettes (borosilicate glass, 2–3 MΩ) were filled with solution containing (in mM): K-gluconate 120, KCl 20, NaCl 5, amphotericin-B 0.44, HEPES 10 (pH 7.2; KOH). Series resistance was compensated by ≥80%, and potentials were corrected for the calculated liquid junction potential. APs were low-pass filtered (cut-off frequency: 2 kHz) and digitized at 10 kHz, and I_f was filtered and digitized at 1 kHz and 4 kHz, respectively. Voltage control, data acquisition and analysis were done with custom software. Cell membrane capacitance (C_m) was estimated by dividing the time constant of the decay of the capacitive transient in response to 5-mV hyperpolarizing voltage clamp steps from −40 mV by the series resistance.

Action potentials measurements. We recorded spontaneous APs, or APs elicited at 1 Hz by 3-ms, ~1.2× threshold current pulses through the patch pipette. APs were characterized by duration at 20%, 50%, and 90% repolarization (APD_{20}, APD_{50}, and APD_{90}, respectively), maximum diastolic potential (MDP), AP amplitude (APA), maximum upstroke velocity (dV/dt_{max}), and, in the case of spontaneously active cells, cycle length (CL) and diastolic depolarization rate measured over the 100-ms time interval starting at MDP + 1 mV (DDR_{100}). Parameter values obtained from ten consecutive APs were averaged.

I_f measurements. I_f was activated upon 2-s hyperpolarizing pulses from a holding potential of −40 mV. I_f amplitude was calculated as the difference between the current at the beginning and end of the voltage step. Current densities were calculated by dividing current amplitudes by C_m.

Statistical analyses. Normality and equal variance assumptions were tested with the Shapiro-Wilk (or Kolmogorov-Smirnov test if N was too small) and the Levene median test, respectively. Groups were compared with unpaired *t*-test or, in case of a failed normality and/or equal variance test, Mann-Whitney rank sum test. A paired *t*-test was used to compare drug effects within a group of cells and cell proliferation from the same starting population. One-way ANOVA with Bonferroni's correction was used to compare the means of multiple groups. $P < 0.05$ was considered statistically significant.

53. Bellin, M. *et al.* Isogenic human pluripotent stem cell pairs reveal the role of a KCNH2 mutation in long-QT syndrome. *EMBO J.* **32**, 3161–3175 (2013).
54. Maherali, N. *et al.* A high-efficiency system for the generation and study of human induced pluripotent stem cells. *Cell Stem Cell* **3**, 340–345 (2008).
55. Birket, M.J. *et al.* PGC-1-α and reactive oxygen species regulate human embryonic stem cell-derived cardiomyocyte function. *Stem Cell Rep.* **1**, 560–574 (2013).
56. Hao, J. *et al. In vivo* structure activity relationship study of dorsomorphin analogs identifies selective VEGF and BMP inhibitors. *ACS Chem. Biol.* **5**, 245–253 (2010).
57. Rape, A.D., Guo, W.-H. & Wang, Y.-L. The regulation of traction force in relation to cell shape and focal adhesions. *Biomaterials* **32**, 2043–2051 (2011).